LETTER OF INTENT
STUDY OF IN-MEDIUM MODIFICATIONS OF ϕ INSIDE THE NUCLEUS WITH $\phi \to K^+K^-$ MEASUREMENT WITH THE E16 SPECTROMETER

(Submitted to the 31st J-PARC PAC meeting on January 20-22, 2020)

H. Sako (*spokesperson*)[1,2], K. Aoki[3], W. C. Chang[4], M. L. Chu[4], T. Chujo[2], S. Esumi[2], M. Inaba[8], Y. Miake[2], M. Naruki[5,1], T. Nonaka[2], K. Ozawa[3,7,2], S. Sato[1], T. N. Takahashi[6], and S. Yokkaichi[6]

[1]Advanced Science Research Center, Japan Atomic Energy Agency, Tokai, Ibaraki 319-1195, Japan
[2]Tomonaga Center for the History of the Universe, University of Tsukuba, Tsukuba, Ibaraki 305-8571, Japan
[3]Institute of Particle and Nuclear Studies (IPNS), High Energy Accelerator Research Organization (KEK), Tsukuba, Ibaraki 305-0801, Japan
[4]Institute of Physics, Academia Sinica, Taipei 11529, Taiwan
[5]Department of Physics, Kyoto University, Kyoto 606-8502, Japan
[6]RIKEN Nishina Center, RIKEN, Wako, Saitama 351-0198, Japan
[7]Department of Physics, University of Tokyo, 7-3-1 Hongo, Tokyo 113-0033, Japan
[8]Division of Industrial Technology, Tsukuba University of Technology, Tsukuba, Ibaraki 305-8520, Japan

December 21, 2020

Abstract

We propose to measure $\phi \to K^+K^-$ decay in p+A collisions with the E16 spectrometer. In this measurement, we study in-medium modification of ϕ properties inside the nucleus with the invariant mass spectrum and the branching ratio. This study is complementary to $\phi \to e^+e^-$ measurement at E16, which is expected to clarify the low-mass tail found in E325. In $\phi \to K^+K^-$ decay, since the ϕ mass is close to the mass threshold of K^+K^-, the branching ratio is sensitive to the subtle change of the ϕ mass. We will measure the branching ratio and the invariant mass spectrum of $\phi \to K^+K^-$ decay, focusing on low velocity range of ϕ, where E325 observed low-mass tail in the invariant mass spectrum of $\phi \to e^+e^-$. We propose the detector configuration for the above measurements including Kaon trigger and identification using trackers, MRPC's and Aerogel Cherencov counters. We request 30-day beam time to collect several 100k $\phi \to K^+K^-$ decays.

Contents

1 Introduction and Goals

In dense nuclear matter, hadrons are expected to change their properties due to partial chiral symmetry restoration. In order to study modification of ϕ mass in the nuclear matter, we will measure $\phi \to K^+K^-$ decay in proton-nucleus (p+A) collisions, where slow ϕ is produced inside the nucleus. We measure the invariant mass spectrum and the branching ratio the decay. Since the ϕ mass is very close to the K^+K^- decay threshold, the branching ratio is expected to be sensitive to the change of ϕ mass.

In this LOI, we propose to measure $\phi \to K^+K^-$ decay in p+A collisions at J-PARC E16. This study is complementary to $\phi \to e^+e^-$ measurement at E16. We will measure the branching ratio of $\phi \to K^+K^-$. In particular we focus on low velocity of ϕ, where the produced ϕ has large probability to stay inside the nucleus.

The E325 experiment at KEK-PS [2, 1] is the previous experiment of J-PARC E16 [5], which measured $\phi \to e^+e^-$ and $\phi \to K^+K^-$ in p+A collisions. E325 observed a low mass tail at the ϕ peak in the e^+e^- invariant mass spectrum in p+Cu collisions at low ϕ velocity ($\beta\gamma < 1.25$). Note that the low mass tail is observed at e^+e^- invariant mass range of $0.94 < m_{inv} < 1.0$ GeV/c^2 which is mostly below the $\phi \to K^+K^-$ invariant mass threshold of 0.987 GeV/c^2. Therefore, the modification may appear in the K^+K^- channel more clearly as the reduction of the cross section rather than the low mass tail. Indeed, no shape modification of the K^+K^-invariant mass spectra was observed in E325.

The E325 results of $\phi \to K^+K^-$ measurement are shown in Fig. 1. The cross section of ϕ is assumed to scale with the target mass number A and the α parameter as,

$$\sigma_{pA}(c) = \sigma_{pp}(c)A^{\alpha}, \tag{1}$$

where c shows each decay channel of $\phi \to K^+K^-$ or $\phi \to e^+e^-$, The α parameter is obtained with C and Cu targets as follows;

$$\alpha(c) = \frac{\ln\left(N_c(A_1)/N_c(A_2)\right)}{\ln\left(A_1/A_2\right)}, \tag{2}$$

and A_1 and A_2 is the mass numbers of Cu and C, respectively.

The difference of α between $\phi \to K^+K^-$ and $\phi \to e^+e^-$ is related to the ratio of the two decay yields $R = N_{K^+K-}/N_{e^+e^-}$ as follows;

$$\Delta\alpha = \alpha(K^+K^-) - \alpha(e^+e^-) = \frac{\ln\left(R(A_1)\right)/\ln\left(R(A_2)\right)}{\ln\left(A_1/A_2\right)}. \tag{3}$$

If $R(A)$ with larger A (Cu) changes with respect to that with small A (C) due to larger nuclear density effect, $\Delta\alpha$ also changes accordingly. However, $\Delta\alpha$ was consistent with zero (namely $R(A)$ did not change between two targets) within statistical uncertainties, although slight increase towards low $\beta\gamma$ was observed in the bottom right plot of Fig. 1.

However, it is clear from Fig. 1 the statistics of E325 is small, in particular at low $\beta\gamma$. It is therefore important to measure $\phi \to K^+K^-$ mainly at low $\beta\gamma$ region with large statistics.

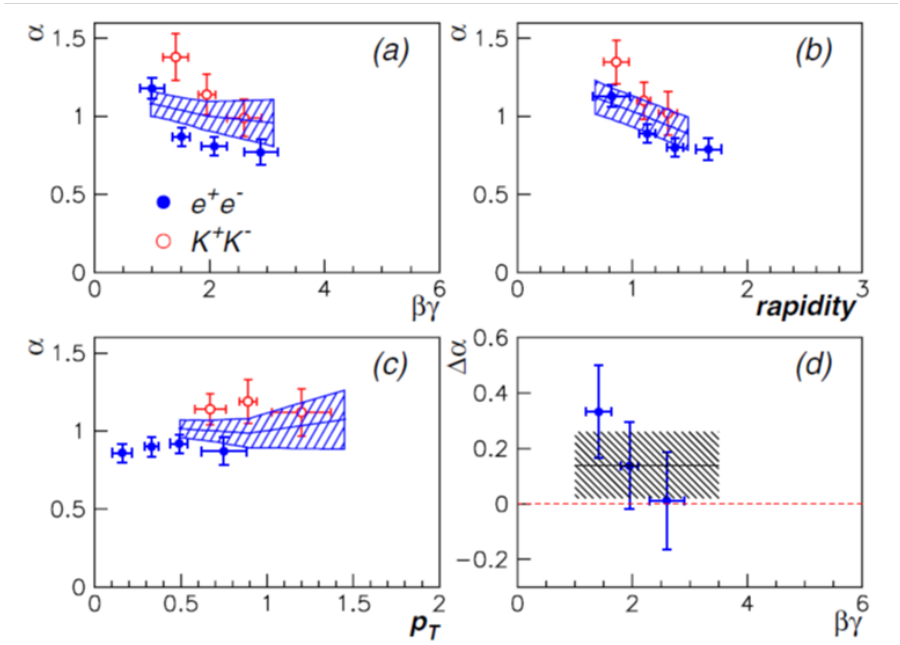

Figure 1: E325 results of $\phi \to K^+K^-$ study are shown [1]. Top left, top right, and bottom left plots show the target nuclear dependence coefficient α as a function of $\beta\gamma$, rapidity, and p_T of ϕ. The bottom right figure shows the difference of α between $\phi \to K^+K^-$ and $\phi \to e^+e^-$ as a function of $\beta\gamma$.

Two strategies can be considered for $\phi \to K^+K^-$ measurements.

1. Systematic measurements in the wide $y-p_T$ acceptance to have large acceptance overlap with $\phi \to e^+e^-$.

2. Focus on low $\beta\gamma$ acceptance where a low mass tail in the invariant mass spectrum of $\phi \to e^+e^-$ observed.

In this LOI, we take Strategy 2. We use Aerogel Cherenkov counter (AC) to veto high-momentum pion background in the trigger level as shown in Fig. 3. For this strategy, we set the refractive index of AC to be a large value (1.26), which is the maximum index aerogel available in Japan [8], so that we enhance low $\beta\gamma \leq 1.5$ ϕ.

Strategy 1 is similar to that of E325, where the refractive index 1.034 was used to veto high-momentum pion background as shown in Fig. 3. E325 measured ϕ in rather a wide range of $y - p_T$ and $\beta\gamma$. To make larger overlap with e^+e^- measurement, we further need to cover forward acceptance around the beam axis to measure the mid-rapidity. It may be good also for further systematic studies of hadron production for the physics such as small system flow, and as baseline experiments towards the future

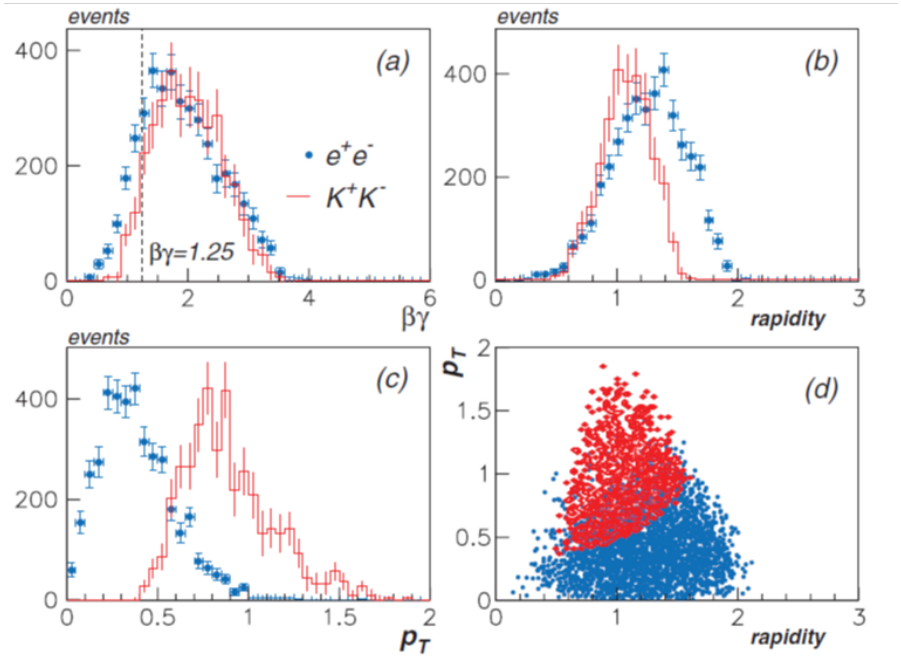

Figure 2: E325 acceptance of $\phi \rightarrow K^+K^-$ and $\phi \rightarrow e^+e^-$ are shown [1]. Top left, top right, and bottom left figures show acceptance in $\beta\gamma$, rapidity, and p_T of ϕ. The bottom right figure shows the acceptance in rapidity-p_T.

heavy-ion collision experiment at J-PARC [7]. Strategy 1 will be investigated in the future.

In this LOI, we propose to measure $\phi \to K^+K^-$ decay focusing on low $\beta\gamma$. At E325, 1.5k $\phi \to K^+K^-$ decays were measured. We propose to collect two-order higher statistics of several-hundred-thousands to observe changes of the branching ratios between the two decay channels.

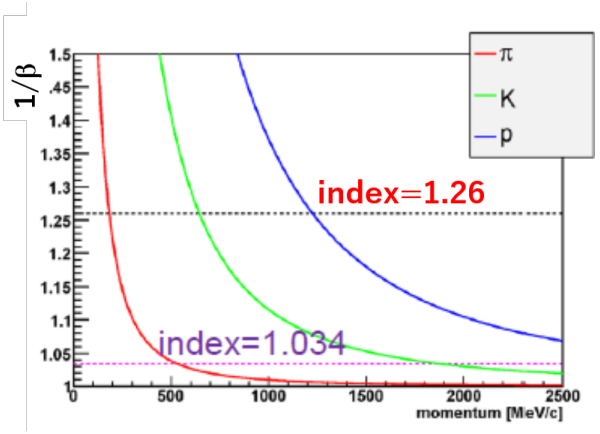

Figure 3: $1/\beta$ as a function of the momentum for π, K, and p. The refractive index of 1.034 is used fin E325 which the LOI uses 1.26.

We consider the following two detector configurations A and AB and evaluated the $y - p_T$ acceptance using GEANT4 simulation with p+A collisions of the JAM model as shown in Figs. 5 and 6. The E16 detector configuration consists of an unit of "module", which has the coverage in θ_x of $\sim 30^o$ and the coverage in θ_y of $\sim 30^o$, where $\theta_x = \tan^{-1}(x/z)$, and $\theta_y = \tan^{-1}(y/z)$, and the z-, x-, y- positions are along with the beam-direction, horizontal, and vertical directions in the left-handed coordinate system with the origin at the target.

The detector configuration and the $y - p_T$ acceptance of $\phi \to e^+e^-$ at Run 0 are shown in Fig. 4 where it covers the mid-rapidity of ~ 1.6.

Configurations A and AB for $\phi \to K^+K^-$ cover backward rapidity regions. By requiring the AC veto with the refractive index of 1.26, the acceptance is further limited to low p_T and backward rapidity as shown in Figs. 5 and 6. The $\beta\gamma$ coverage is $\beta\gamma < 1.5$ by requiring AC veto as shown in Fig. 7.

In this LOI, we propose Configurations A and AB. We first build detectors of Configuration A, and then build additional detectors for Configuration AB. Since they do not conflict with the Run 0 detector configuration for e^+e^- measurements shown in Fig. 4, it is easy to install detectors with minimum interference with other existing detectors, and also it is possible perform beam tests and commissioning with beams during e^+e^- runs. In the physics runs of K^+K^-, we could run with e^+e^- measurements at the same time, while K^+K^- measurements require lower beam intensity than e^+e^-. Still a quick switch between K^+K^- and e^+e^- during the beam period will

be possible.

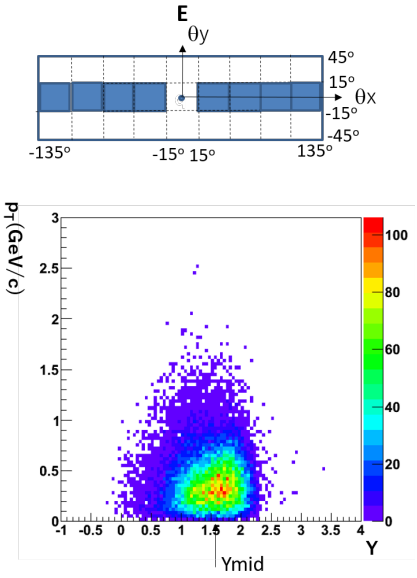

Figure 4: Detector configuration E for $\phi \to e^+e^-$ (top) and its $y - p_T$ acceptance (bottom) at Run 0.

Just for the reference for the above Strategy 1, Configuration AF is also shown in Fig. 8 It has good acceptance overlap with e^+e^- at $0.7 < y < 1.9$ and $0.2 < p_T < 1.5$ GeV/c. At the most forward module around the beam axis, we set the acceptance to be $7.5^o < |\theta_x| < 15^o$ and $7.5^o < |\theta_y| < 15^o$ to avoid the beam particles and the beam halo.

2 Detector Design

The detector setup based on Configuration A is shown in Fig. 9. The E16 spectrometer consists of three vertical layers (top, middle, and bottom), and 8 modules in θ_x [5]. In Run 0 setup for electron measurement, detectors are installed in the 8 modules in the middle layer [6]. For charged particle tracking, the Silicon Strip Detectors (SSD's), three-layer GEM trackers (GTR's) are used. For electron identification, Hadron Blind Detectors (HBD) and Lead-glass Calorimeter (LG) are used.

We use only the top and bottom layers in Configuration A and AB. In the top and bottom layers, we use GTR's in the 6 most-forward modules for A and 18 modules for AB to cover the horizontal angle range of $-45^o < \theta_x < 45^o$ and $-135^o < \theta_x < 135^o$, respectively. We install the start timing counters (Track Start Counter, TSC) at $R \sim 0.1$ m, Aerogel Cherenkov Counters (AC) at $R \sim 1.1$ m, and MRPC's at $R \sim 1.3$ m.

In the following subsections, the detector design and prototype R&D status of the new detector for $\phi \to K^+K^-$ measurements will be described.

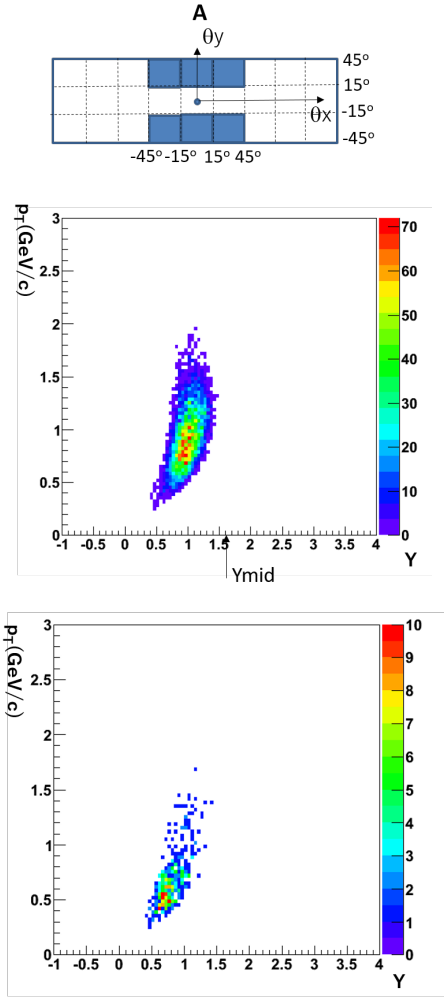

Figure 5: Detector configuration A (top), its $y - p_T$ acceptance (middle), and the acceptance requiring AC veto with the index of 1.26 (bottom).

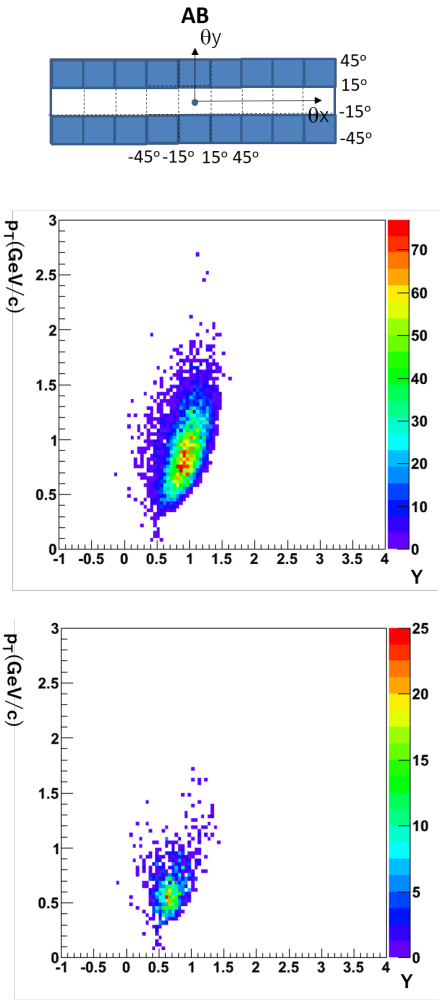

Figure 6: Detector configuration AB (top), its $y - p_T$ acceptance (middle), and the acceptance requiring AC veto with the index of 1.26 (bottom).

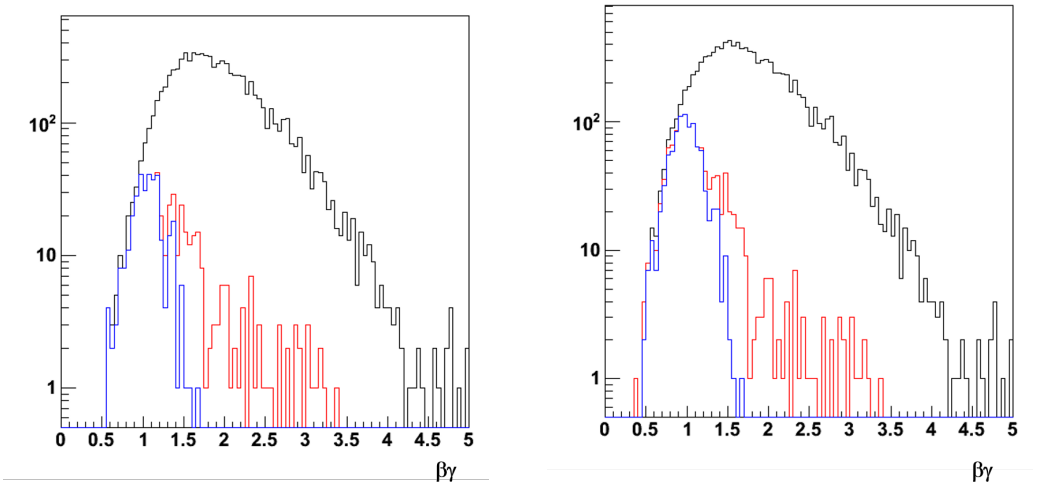

Figure 7: The $\beta\gamma$ distributions of ϕ for Configurations A (left) and AB (right). The black lines are without selection, red lines are with AC veto, and blue lines are with the unlike-sign track trigger described below.

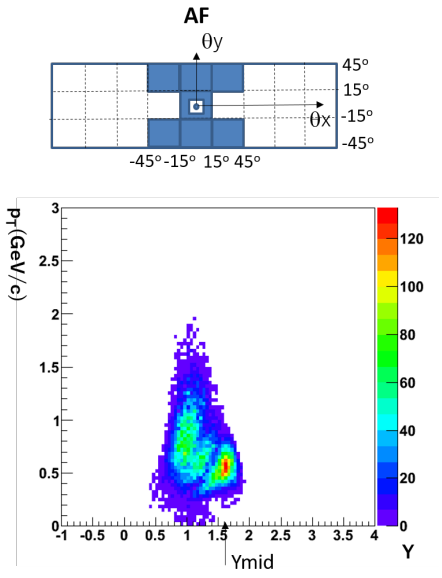

Figure 8: Detector configuration AF (top) and its $y - p_T$ acceptance (bottom)requiring AC veto with the index of 1.034.

3 Experimental Setup

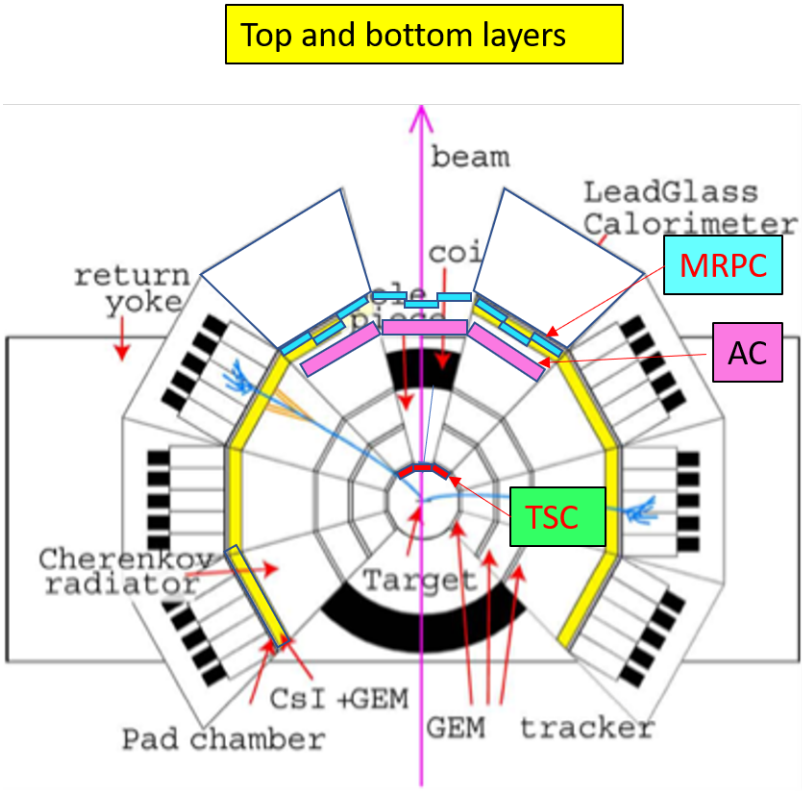

Figure 9: The detector setup in Configuration A in the top and bottom layers.

3.1 Multi-gap Resistive Plate Chamber (MRPC)

In order to identify charged Kaons, MRPC is used for high-resolution time-of-flight measurement. Fig. 10 shows the expected particle identification performance assuming the TSC and MRPC timing resolution of 50 ps and 60 ps with the path length of 1.2 m, respectively. We are developing an MRPC based on that of BGOegg experiment [3]. The structure of the MRPC is shown in Fig. 11. It consists of an anode PCB in the middle, and cathode PCB's in the top and bottom. Between top and bottom cathode PCB's, there are 10 gas gap of 120 μm made of 12 sheets of glass. About $\pm$7kV is applied on the top and bottom cathode electrodes while the anode electrode is grounded so that electron avalanche is produced in the gas gaps when a charge particle passes through. The electrodes are made of high-resistive carbon sheets. The MRPC has 8 readout strips in the anode PCB with the dimension of $26\mathrm{mm} \times 770\mathrm{mm}$ as shown in Fig. 12. We constructed a prototype MRPC and tested it with LEPS beamline in Nov. 2020. In the preliminary analysis we obtained the detector efficiency of

$97 \pm 1\%$ and 72 ± 1 ps without slewing corrections, respectively. The resulting TOF resolution and TOF vs TOT correlation are shown in Fig. 14 and 15.

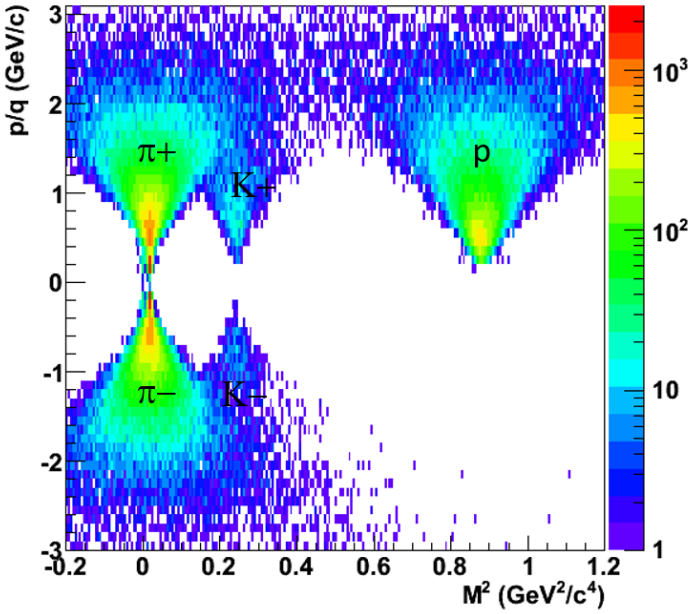

Figure 10: Simulated rigidity (GeV/c) as a function of squared mass (GeV/c^2) assuming the TSC and MRPC timing resolution of 50 ps and 60 ps with the path length of 1.2 m, respectively.

3.2 Track Start Counter (TSC)

Track Start Counter (TSC) is the start timing counter for the time-of-flight measurement with MRPC, which is segmented plastic scintillation counter. A prototype TSC consists of eight segments of $4\ \mathrm{mm} \times 4\ \mathrm{mm} \times 100\ \mathrm{mm}$ plastic scintillator, where scintillation light is detected with MPPC with $3\ \mathrm{mm} \times 3\ \mathrm{mm}$ sensitive area. In the test with a beta-ray source, we obtained the timing resolution of 55 ± 5 ps.

3.3 Aerogel Cherenkov Counter (AC)

Aerogel Cherenkov Counter (AC) is used to veto fast pion background in the trigger. The AC prototype was developed with the aerogel radiator with the refractive index of 1.034, with fine-mesh PMT of 3-inch diameter for photon detection. Since AC is used inside the magnetic field of the E16 spectrometer, a fine-mesh PMT is required. Its design and photograph is shown in Figs. 17 and 18 [4].

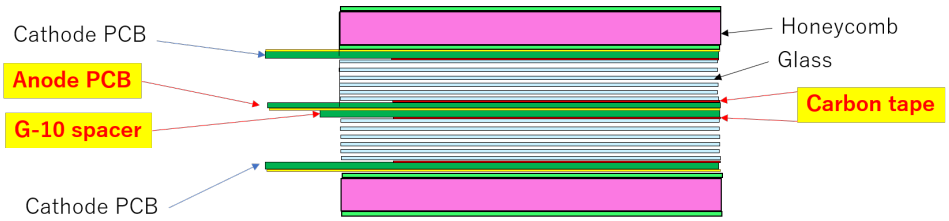

Figure 11: The MRPC structure.

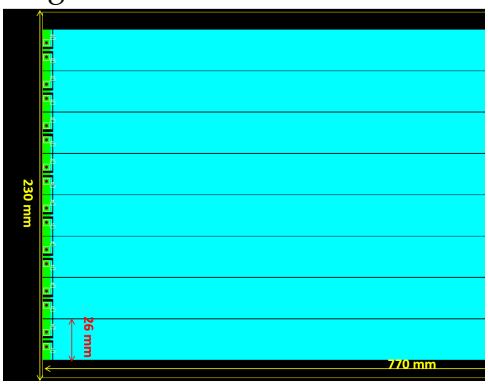

Figure 12: The MRPC anode PCB design.

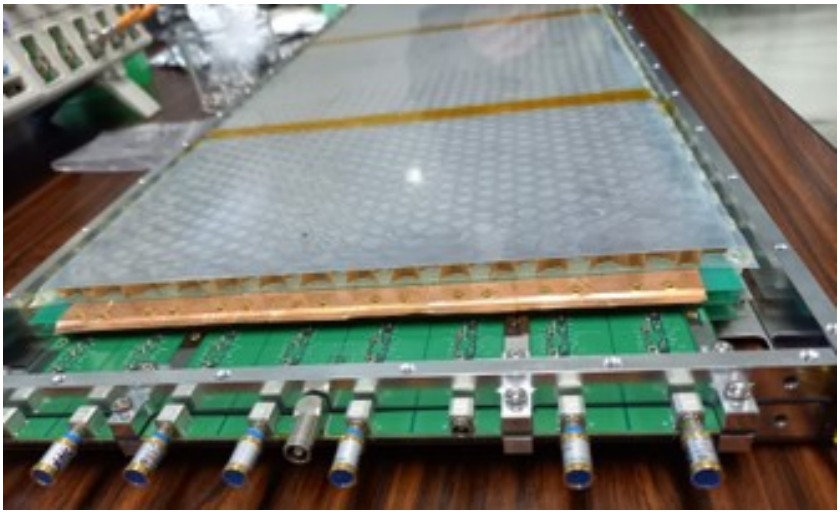

Figure 13: A photograph of an MRPC prototype.

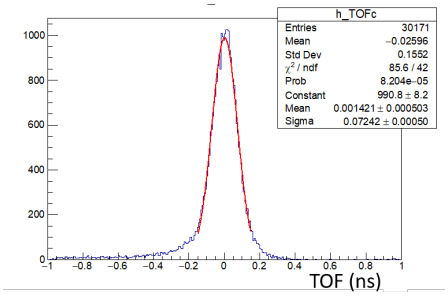

Figure 14: The measured TOF distribution of electron beams of light velocity.

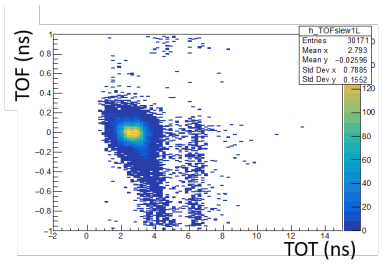

Figure 15: The measured TOF as a function of Time-Over-Threshold (TOT) of electron beams.

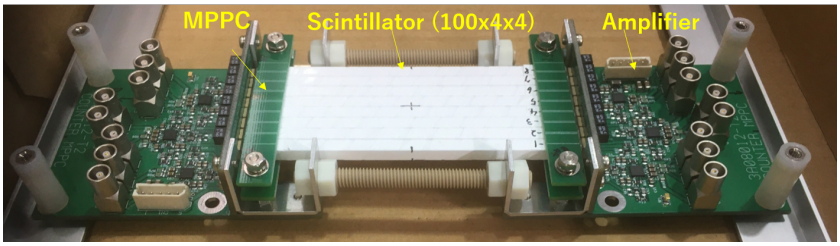

Figure 16: A photograph of a TSC prototype.

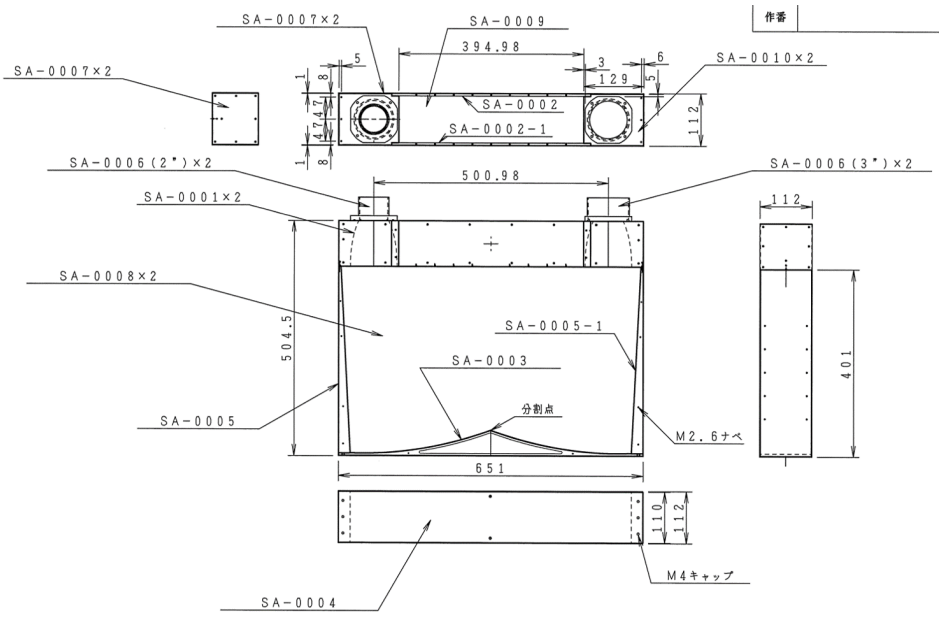

Figure 17: The design of the AC prototype.

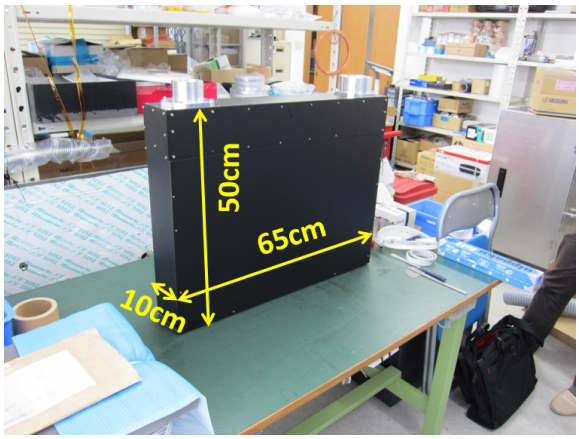

Figure 18: A photograph of the AC prototype.

3.4 Trackers

In the top and bottom layers, we adopt as trackers the same GTR's as being used for electron measurements.

4 Expected results

We describe here the definition of the triggers, and evaluate the performance of the trigger, Kaon identification, and the invariant mass spectra of K^+K^- in the simulation.

We define the triggers as below, based on those used in E325. The "Unlike-sign" trigger is to select two unlike-charge particles and reject high-momentum charge particles using TSC slat and MRPC strip information. The "KK" trigger is to select K^+K^-.

1. Unlike-sign trigger
   (a) Require at least 2 MRPC hits with AC veto
   (b) Require a pair of unlike-sign charge particles using MRPC strip - TSC slat relation
   (c) Reject high-momentum tracks with MRPC strip – TSC slat relation
2. KK trigger
   (a) Require Unlike-sign trigger defined above
   (b) Cut using the relation among the time of flight (TOF) between TSC and MRPC, TSC slat, and MRPC strip to select tracks consistent with $K^{\pm}$.

We use AC with the refractive index of 1.26. The inverse of the velocity as a function of momentum is shown in Fig. 3. The momentum threshold above which Cherenkov light is emitted is about 0.2 GeV/c, 0.6 GeV/c, and 1.2 GeV/c for π, K, and p, respectively. We assume the AC efficiency to be 90 % above the velocity threshold of 0.794, and 8 % below the threshold, which are the values of the E325 AC.

Fig. 19 shows the horizontal hit position $R\theta_x$ of MRPC as a function of that of TSC with AC vetoed tracks, where $R = \sqrt{x^2 + z^2}$ and $\theta = \tan^{-1}(x/z)$. It includes the information of both the initial track angle and the deflection depending on its momentum.

In order to suppress the effect of the initial track angle, we redefine a variable which is a measure of the track deflection as;

$$\Delta R\theta_x = R\theta_x(\mathrm{MRPC}) - aR\theta_x(\mathrm{TSC}), \tag{4}$$

where Parameter a is obtained by the straight-line fit to the p distribution.

The resulting corrected horizontal position $\Delta R\theta_x$ is shown in Fig. 20. It is flat as a function of the TSC position. To reject tracks with small position deflection (namely high momentum), we apply the cut shown as red boxes.

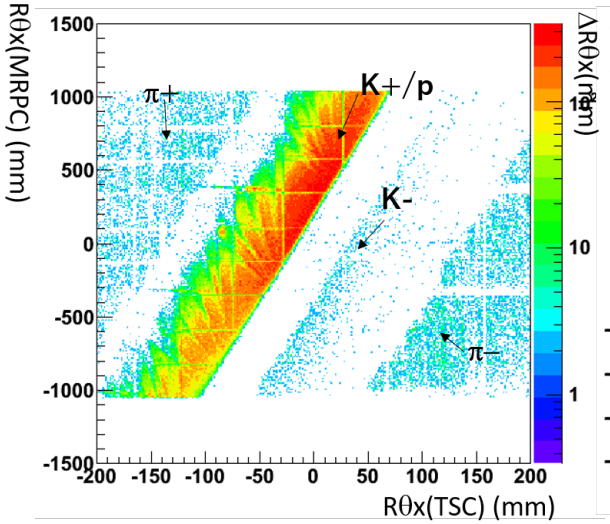

Figure 19: The horizontal hit position $R\theta_x$ of MRPC as a function of that of TSC for all of the particles.

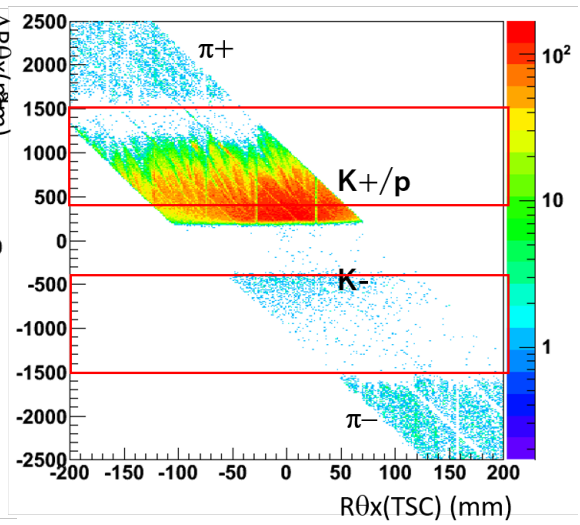

Figure 20: The corrected horizontal hit position $\Delta R\theta_x$ of MRPC as a function of the TSC horizontal hit position $R\theta_x$ for all of the particles.

The cuts are determined by looking at $\Delta R\theta_x$ for each particle shown in Figs. 21, 22, and 23. The plots reflect the track position deflection from TSC to MRPC depending on their rigidity distributions. π has larger ΔR_{θ_x} than K and p, due to lower momentum with AC veto.

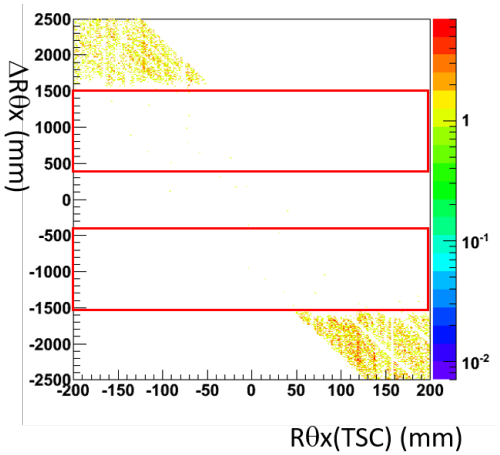

Figure 21: The corrected horizontal hit position $\Delta R\theta_x$ of MRPC with AC veto as a function of the horizontal hit position of TSC $R\theta_x$ for $\pi^{\pm}$.

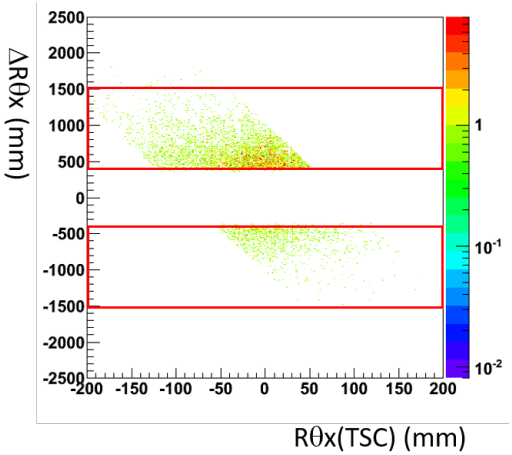

Figure 22: The corrected horizontal hit position $\Delta R\theta_x$ of MRPC with AC veto as a function of the horizontal hit position of TSC $R\theta_x$ for $K^{\pm}$.

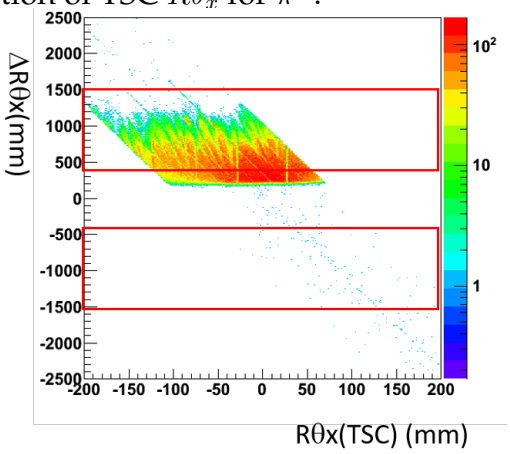

Figure 23: The corrected horizontal hit position $\Delta R\theta_x$ of MRPC with AC veto as a function of the horizontal hit position of TSC $R\theta_x$ for p.

The Kaon selection trigger using the relation between $\Delta R\theta_x$ and TOF between TSC and MRPC is simulated in Fig. 24. The Kaon selection cut is defined as the two parallelograms, which is used for the KK trigger selection.

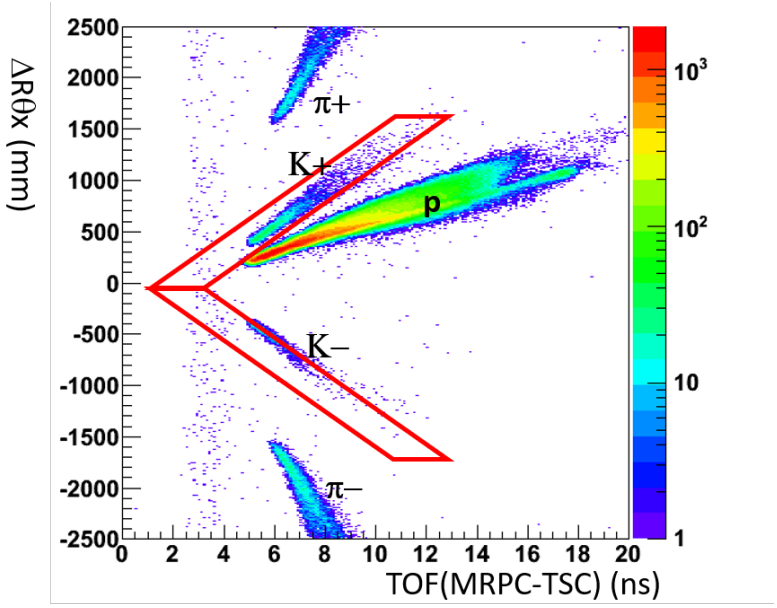

Figure 24: The corrected hit position in $R\theta$ of MRPC as a function of TOF between TSC and MRPC.

Figs. 25 and 26 show the invariant mass spectra in p+Cu and p+Pb simulated in GEANT4 with the JAM model using the trigger selections described above. These plots include background due to mis-identified Kaons due to finite AC efficiency.

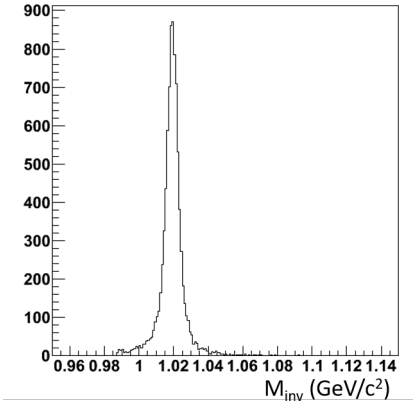

Figure 25: The invariant mass spectrum of K^+K^- with 1M JAM p+Cu events.

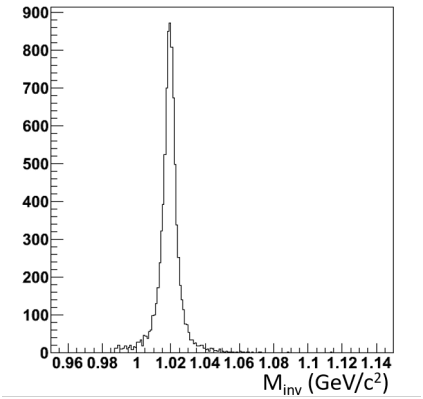

Figure 26: The invariant mass spectrum of K^+K^- with 1M JAM p+Pb events.

5 Beam Time Request

Trigger rates and true $\phi \to K^+K^-$ rates in GEANT4 simulation with JAM model are summarized in Table 1 in p+Cu and Table 2 in p+Pb for Configurations A and AB.

Table 1: The trigger rates and true $\phi \to K^+K^-$ rates in Configurations A and AB in p+Cu.

	Conf. A	Conf. AB
Unlike-sign Trigger	$(1.9 \pm 0.1) \times 10^{-3}$	$(8.6 \pm 0.2) \times 10^{-3}$
KK trigger	$(1.7 \pm 0.8) \times 10^{-5}$	$(5.0 \pm 1.4) \times 10^{-5}$
$\phi \to K^+K^-$	$(2.9 \pm 0.4) \times 10^{-6}$	$(7.3 \pm 0.6) \times 10^{-6}$

Table 2: The trigger rates and true $\phi \to K^+K^-$ rates in Configurations A and AB in p+Pb.

	Conf. A	Conf. AB
Unlike-sign Trigger	$(4.8 \pm 0.1) \times 10^{-3}$	$(1.93 \pm 0.02) \times 10^{-2}$
KK trigger	$(2.3 \pm 0.7) \times 10^{-5}$	$(9.6 \pm 1.4) \times 10^{-5}$
$\phi \to K^+K^-$	$(5.3 \pm 0.8) \times 10^{-6}$	$(1.6 \pm 0.1) \times 10^{-5}$

Then, for Configurations A and AB, we estimated $\phi \to K^+K^-$ yields in 30-day beam time as shown in Tables 3 and 4. We assume the proton beam rate to be 1×10^9 per spill, which is 10 times lower than the beam rate for $\phi \to e^+e^-$ of 1×10^{10}. The target thickness (Cu or Pb) is assumed to be 0.2% interaction length, respectively. The resulting interaction rate is 1×10^6 Hz in the flat top of 2 s with the period of 5.52 s. In E325, there was a factor of 10 higher first-level trigger rate than that estimated in the simulation, which is attributed to the background tracks due to beam halo. This factor 10 is applied to our realistic KK trigger rate in Tables 3 and 4 to the simulated rates in Tables 1 and 2. We also corrected for the ϕ production cross section of the JAM model to the experimental data for p+Cu and p+Pb. We assume the maximum data-acquisition (DAQ) rate to be 1 kHz. The resulting $\phi \to K^+K^-$ yields in 30-day beamtime assuming 10% efficiency are shown as the final estimated $\phi \to K^+K^-$ yields in the right-most column, where the efficiency includes the efficiency of triggers, DAQ, detectors, and offline analyses. In p+Cu and p+Pb collisions with 0.2 % interaction-length targets, we estimate 190k and 520k in Configuration A, and 490k and 1.0M in Configuration AB, respectively. Note the numbers depends strongly on the DAQ rate and the efficiency, and we need to evaluate them more precisely in R&D of the DAQ system and detectors in the proposal.

Also note that there are a few points which have not yet studied in the simulation. We have not considered the effects of fake tracks due to beam halo and decay particles. We also have not considered the overkill problems due to finite segmentation of AC in the forward angles. Those effects will be studied in detail for the experimental proposal.

Table 3: KK trigger rates and expected ϕ yields in 30-day run with Configuration A. "Rate(/ev)","Rate(/d)", "Rate(/30d)", and "10%eff Rate(/30d)" denote the trigger and ϕ rates per event, per day, per 30 days, and per 30 days with 10% efficiency, respectively.

	Rate(/ev)	Rate(/s)	Rate(/d)	Rate(/30d)	10%eff Rate(/30d)
p+Cu (trig)	1.7×10^{-4}	170	5.2M	160M	
p+Cu (ϕ)	2.1×10^{-6}	2.1	65k	1.9M	190k
p+Pb (trig)	2.3×10^{-4}	230	7.2M	220M	
p+Pb (ϕ)	5.5×10^{-6}	5.5	170k	5.2M	520k

Table 4: KK trigger rates and expected ϕ yields in 30-day run with Configuration AB. "Rate(/ev)","Rate(/d)", "Rate(/30d)", and "10%eff Rate(/30d)" denote the trigger and ϕ rates per event, per day, per 30 days, and per 30 days with 10% efficiency, respectively.

	Rate(/ev)	Rate(/s)	Rate(/d)	Rate(/30d)	10%eff Rate(/30d)
p+Cu (trig)	5.0×10^{-4}	500	16M	470M	
p+Cu (ϕ)	5.2×10^{-6}	5.2	160k	4.9M	490k
p+Pb (trig)	9.6×10^{-4}	960	30M	900M	
p+Pb (ϕ)	1.1×10^{-5}	11	350k	10M	1.0M

6 Summary

In this LOI, we propose to study modification of ϕ mass inside the nucleus, which is related to partial chiral symmetry restoration, through $\phi \to K^+K^-$ measurements at E16. We measure invariant spectra and branching ratios of K^+K^- in 2-order higher statistics than E325. This study is complementary to $\phi \to e^+ + e^-$ measurements at J-PARC E16, and E325 where a low-mass tail at the $\phi \to e^+ + e^-$ peak in the invariant mass spectrum was observed at low ϕ velocity in p+Cu. We propose to measure $\phi \to K^+K^-$ yields in the horizontal angles from -45^o to 45^o in the top and

bottom layers as the first stage, and then -135^o to 135^o in the second stage. We introduce Kaon identification detectors, Aerogel Cherenkov counter, MRPC and the start counter (TSC) for these measurements. We expect to have $190\mathrm{k} \sim 1.0\mathrm{M}$ of $\phi \to K^+K^-$ decays in 30-day beam time at 1.0×10^9 / spill proton beam with 0.2 % interaction-length Cu and Pb targets, assuming 1kHz DAQ rate and 10% efficiency.

References

[1] F. Sakuma *et al.*, Phys. Rev. Lett. **98** (2007) 152302.

[2] R. Muto *et al.*, Phys. Rev. Lett. **98** (2007) 042501.

[3] N. Tomida *et al.*, JINST **11** C11037 (2016).

[4] F. Sakuma, E16 internal presentation in Aug. 2011.

[5] S. Yokkaichi *at al.*, J-PARC proposal No. 16 `http://j-parc.jp/researcher/Hadron/en/pac_0606/pdf/p16-Yokkaichi_2.pdf`, Lec. Notes. Phys. **781** (2009) 161-193.

[6] S. Yokkaichi *at al.*, J-PARC E16 Run0 Proposal, `http://j-parc.jp/researcher/Hadron/en/pac_1707/pdf/E16_2017-10.pdf`.

[7] H. Sako, *et al.*, Letter-Of-Intent of J-PARC-HI, `https://j-parc.jp/researcher/Hadron/en/pac\_1607/pdf/LoI\_2016-16.pdf`.

[8] M. Tabata, `http://jahep.org/hepnews/2019/19-4-3-aerogel.pdf` (in Japanese).